JTTEE5 15:640-651
DOI: 10.1361/105996306X147081
1059-9630/$19.00 © ASM International

Peer Reviewed

Effects of Ce and Si Additions to CoNiCrAlY Bond Coat Materials on Oxidation Behavior and Crack Propagation of Thermal Barrier Coatings

K. Ogawa, K. Ito, T. Shoji, D.W. Seo, H. Tezuka, and H. Kato

(Submitted February 24, 2006; in revised form July 17, 2006)

In thermal barrier coating (TBC) systems, thermally grown oxide (TGO) forms at the interface between the top coat and the bond coat (BC) during service. Delamination or spallation at the interface occurs by the TGO formation and growth. Therefore, modifications of the BC materials are one means to inhibit the TGO formation and to improve the crack resistance of TBCs. In this study, morphologies of TGO were controlled by using Ce and Si additions to conventional CoNiCrAlY BC material. The evaluation of the crack resistance was carried out using acoustic emission methods under pure bending conditions. As a result, when the BCs of TBCs with Ce added were aged at 1373 K over 10 h, the morphologies of the TGO were changed drastically. The BC materials of TBCs coated with Ce added indicated an improved crack resistance with high-temperature exposure. It is expected that the morphologies can improve the crack resistance of TBCs.

Keywords cerium, crack resistance, silicon, thermal barrier coatings, thermally grown oxide

1. Introduction

In recent years, due to the demand for saving energy and reducing greenhouse gases, high-efficiency power generation plants have been developed. In power-generating gas turbine plants, improvements in efficiency have been achieved by increasing turbine inlet gas temperature. Hot-section components, such as combustors, rotating blades, and vanes, are exposed to high-temperature environments for prolonged periods of time. Accordingly, the materials for these components require resistance to oxidation and sulfurization at high temperatures. Therefore, thermal barrier coatings (TBC) are important components of advanced gas turbines that require high reliability and endurance (Ref 1, 2). A typical duplex TBC consists of a 100 μm thick metallic *M*CrAlY (M is Ni, Co, or a combination of both) alloy bond coat (BC) and a 250 to 300 μm thick ceramic top coat (TC). The BCs, which function to improve bonding strength and high-temperature corrosion resistance, are mainly produced by low-pressure plasma spraying (LPPS). Generally, partially yttria-stabilized zirconia (YSZ) has been used for TCs, which are mainly produced by air plasma spray (APS). When the turbine blades and combustors are exposed to high temperatures for long periods of time, it is highly probable that critical failure of TBCs, such as cracking, delamination, or spalling, might occur. Improvement of crack propagation resistance is one significant way to improve the reliability of TBCs over the long term.

During exposure to high temperatures, thermally grown oxide (TGO) forms at the interface between the ceramic TC and the metallic BC. The TGO layer of a plasma-sprayed TBC consists of two layers, one is an Al_2O_3 layer, and the other is a mixed oxide layer that consists of NiO, CoO, Cr_2O_3, or $(Ni,Co)(Cr,Al)_2O_4$ spinel oxide (Ref 3). It is generally accepted that the formation of TGO accelerates TBC failures, and the bonding strength of the TBCs is reduced by the growth of TGO (Ref 4, 5). Ogawa et al. (Ref 3) reported that the formation of porosity in a mixed oxide caused the stress concentration sites and a decrease in bonding strength. Therefore, the inhibition of TGO formation, especially the inhibition of mixed oxide formation, would be an effective means for improving the bonding strength or the resistance to crack propagation. It has been reported that the TGO growth rate depends on, for example, chemical composition, the existence of atomic order defects in the BC, and TC materials (Ref 4, 6). Some approaches, such as modification of the BC or of the coating processes, along with optimization of the coating conditions to inhibit the formation of TGO have been considered.

In the 50+ years since the reactive element (RE) effect was patented, a vast amount of research has been conducted on this phenomenon. Yet, there is still little agreement, not only about what the effect is, but, more importantly, about how a small addition of an oxygen RE can have such a profound effect on the oxidation behavior of chromia- and alumina-forming alloys. It has been shown that arguments that the RE effect is too complex

This article was originally published in *Building on 100 Years of Success: Proceedings of the 2006 International Thermal Spray Conference* (Seattle, WA), May 15-18, 2006, B.R. Marple, M.M. Hyland, Y.-Ch. Lau, R.S. Lima, and J. Voyer, Ed., ASM International, Materials Park, 2006.

K. Ogawa, K. Ito, T. Shoji, and **D.W. Seo,** Fracture and Reliability Research Institute, Tohoku University, Aoba 6-6-01, Aramaki, Aoba-ku, Sendai 980-8579, Miyagi, Japan; and **H. Tezuka,** and **H. Kato,** Tokyo Electric Power Company, Yokohama, Kanagawa, Japan. Contact e-mail: kogawa@rift.mech.tohoku.ac.jp.

to explain with one all-encompassing theory are not necessary. Also, it has been argued that in establishing models of the RE effect it is artificial to postulate substantial differences between chromia and alumina scales. Both chromia and alumina scales are dense, relatively slow-growing, and protective, and both are profoundly affected by the addition of small amounts of certain elements or their oxides. When properly doped, both αCr_2O_3 and $\alpha A1_2O_3$ change from buckled, void-filled, poorly adherent scales to flatter, denser, more adherent, and thus more protective scales. A standard list of RE effects would include: (a) an improvement in scale adhesion or resistance to spallation; (b) a change in the scale-growth mechanism; (c) a reduction in the oxidation rate, related to this change in mechanism; and (d) a modification of the scale microstructure. A fifth effect that has been deliberately omitted is an improvement in selective oxidation in chromia formers. Thus, as defined here, there are only three separate effects because items (b) and (c) above are essentially the same; a reduction in the macroscopic growth rate is the result of a change in the oxidation mechanism.

The study of the RE effect has advanced quickly over the last decade mainly due to the introduction and application of more advanced analytical techniques, such as secondary ion mass spectroscopy, scanning auger microscopy, and field-emission gun scanning transmission electron microscopy, which has allowed the examination of a potential RE mechanism to move closer to the atomic level. The results of experiments using these techniques have significantly advanced the understanding of the RE effect to the point where a comprehensive theory can be proposed.

The authors' research team developed the modified BC materials by adding Ce and Si to the conventional materials (Ref 7). As a result, they succeeded in producing a TBC with four-point bending (FPB) strength that is three times higher than that for the conventional TBC. However, the authors had not considered the optimal chemical composition of Ce and Si added to CoNiCrAlY BC materials. In this study, to further the improvement of the resistance to crack propagation, chemical compositions of CoNiCrAlY with Ce and Si (CoNiCrAlYCeSi) powders are investigated.

2. Reactive Element Effect

It is known that scale spallation is a serious problem, especially for many high-temperature components, which have very close tolerances. In such cases, material loss due to scale spallation will not only create unnecessary vibrations, but also debris of the scale may clog the pipes or cause wear and erosion of the component. Hence, it is imperative to know suitable preventive methods. One of the simplest ways to control scale spallation is to choose a material that forms thin scales that have thermal coefficients of expansion that are close to those of their respective metals. However, this is not always possible. In 1937, Griffiths and Pfeil demonstrated that rare earths added as a melt deoxidant to Ni-20Cr alloys had a beneficial effect on their lifetime when used as heating elements under thermal cycling conditions. These empirical observations were applied later by Pfeil to develop surface treatments with rare earth salts or oxides to enhance the corrosion and oxidation resistance of refractory alloys without affecting their creep properties. According to him, the beneficial effect was observed for different levels of doping with chemical elements belonging to groups II, III, IV, and V of the periodic table. The extent of the benefit was found to decrease from group II to V but increased with the atomic weight in the given group. According to his studies, he found that only some elements in these groups have practical importance.

The so-called REs belong to the rare earth group in the periodic table. Elements such as Y, Ce, La, and Hf have a strong affinity for oxygen. However, there is no single mechanism that can suitably explain the role of REs in combating scale spallation; instead, several mechanism have been put forward, acting either alone on a specific system or in various combinations, to explain the reasons for improvement in the oxidation behavior. The beneficial effects of RE are currently regarded as being of two kinds, an improvement in oxide-to-metal adhesion, and a reduction in the oxidation rate for some systems. The first effect occurs quite widely and is particularly important for alloys that form alumina scales. The second effect is not seen for alumina formers but is important for scales growing by the outward diffusion of cations through the oxide. This is particularly important for alloys that form chromia scales. The most common REs that cause a beneficial effect on oxidation behavior are yttrium, hafnium, cerium, and lanthanum or oxide dispersoids of these elements. An RE can have a detrimental or beneficial influence, depending on its amount and distribution, the alloy composition, and the impurity content. For example, it has been found that the presence of titanium and zirconium has a deleterious effect on the alumina scales when these elements are present along with yttrium. It has also been found that REs like Y can modify the scale adherence for metals/alloys having tramp element impurities such as sulfur. An RE can be incorporated into or onto the metallic substrate in many ways: by the addition of pure RE or an alloy; as an oxide dispersion; or by various surface coating, such as ion implantation or laser surface alloying.

There are various mechanisms by which the role of RE has been explained to cause a beneficial effect to the scale adhesion or to the scale growth process. The following represent some of the theories proposed in the last three decades on the basis of certain specific experimental evidence: (a) REs can promote the nucleation of alumina and consequently reduce the aluminum content necessary to form a continuous protective alumina scale; (b) they can form an intermediate oxide scale that acts as a diffusion barrier for the outward transport of metal ions; (c) the presence of an RE can reduce the accumulation of voids at the oxide-alloy interface because they are well known as vacancy sinks, thereby enhancing the scale adherence; (d) the presence of an RE can result in the formation of pegs that act as mechanical keying between the scale and the substrate; (e) the presence of REs can modify the morphology and microstructure of the scale; (f) change in the growth mechanism of the scale, in the case of alumina, has been found that the presence of REs can change the growth mechanism from the outward movement of aluminum ions to the inward movement of oxygen ions, which results in better scale adherence; (g) modification in the mechanical properties of the scale such as oxide plasticity; and (h) the presence of REs can cause enhanced bond strength by eliminating impurities such as sulfur at the alloy-oxide interface with segregation of sulfur at grain boundaries. This is also known as the sulfur effect.

Several common features emerge from the discussion of the RE effects on Cr_2O_3 scale establishment, growth and failure.

Table 1 Nominal chemical composition and particle size range of spraying powders

Powder type	Designation	Chemical composition(a), wt.%							Particle size, μm			
		Co	Ni	Cr	Al	Y	Ce	Si	Analyzed range	Mean	SD	SE
CoNiCrAlY	CoNiCrAlY	bal	32	21	8	0.5	…	…	−34.2 + 3.8	11.9	6.8	0.96
CoNiCrAlYCe	0.5Ce	bal	32	21	8	0.5	0.5	…	−47.9 + 1.4	15.7	13.2	1.86
CoNiCrAlYSi	1Si	bal	32	21	8	0.5	…	1	−34.8	14.5	8.8	1.21
	0.5CelSi	bal	32	21	8	0.5	0.5	1	−43.8 + 2.8	12.9	9.7	1.37
	1Ce1Si	bal	32	21	8	0.5	1	1	−47 + 1.9	19.3	10.7	1.48
CoNiCrAlYCeSi	1.5Ce1Si	bal	32	21	8	0.5	1.5	1	−45.1 + 2.9	13.3	8.8	1.23
	0.5Ce2Si	bal	32	21	8	0.5	0.5	2	−32.5 + 2.7	15.6	8.2	1.16

(a) Specified by supplier

The effects derive from the provision of RE oxide particles, which act as heterogeneous nucleation sites at the alloy surfaces, as sources of RE ionic segregation to block fast diffusion paths in the scale, as inhibitors of grain growth, as promoters of improved scale mechanical properties, and as sites for crack arresting. Several factors can be identified as maximizing their influence. The first is the desirability of oxide particle formation from the onset of oxidation. The second is a smaller particle size provides a high grain boundary segregant concentration and avoids the direct initiation of scale failure, which is possible with large particles. A third factor is a dense uniform particle distribution provides many sites for particle-related mechanisms and close overlap between regions of high segregant concentration around particles. These characteristics will be influenced by the identity and quantity of the RE, and by the form of its distribution (e.g., alloying addition, oxide dispersion, surface oxide coating, or implant) prior to oxidation.

3. Materials and Experimental Procedures

The substrate material selected in this study was commercially available Inconel 601, which is widely used for gas turbine components. The nominal chemical composition of the substrate material was 59Ni-22Cr-1.3Al-0.2Si-0.2Mn-0.1Cu-0.1C-balance Fe and of 4.0 mm thickness. The substrates were polished and grit blasted with alumina (Al_2O_3) powder before being plasma sprayed, and then positioned into an LPPS coating system to overlay several kinds of BCs to approximately 100 μm thickness, and the same process conditions were applied to all samples. A YSZ (8 wt.% Y_2O_3) (204NS; Sulzer Metco, Winterthur, Switzerland) TBC TC approximately 300 μm thick was then applied using an APS coating system. Six different Ce- and/or Si-added BC materials were developed. The commercial spraying powder CoNiCrAlY (AMDRY 9951; Sulzer Metco) was selected as a basic spraying powder. Other modified powders were specially ordered from the manufacturer with the content control of REs (i.e., Ce and Si). The basic CoNiCrAlY powder has a nominal composition of balance Co32wt.%Ni-21wt.%Cr-8wt.%Al-0.5wt.%Y, whereas the modified powders have additional compositions of 0-1.5wt.%Ce and 0-2.0wt.%Si. These Ce- and/or Si-added BC materials were compared with a conventional CoNiCrAlY. All powders were manufactured by the gas atomization method and exhibited a near-spherical morphology, as shown in Fig. 1. Table 1 shows the classification of the powders, and their nominal chemical compositions and particle size ranges. From Table 1, six special-ordered CoNiCrAlY-Ce and CoNiCrAlY-Se powders of similar size range, from several micrometers to over 48 μm, were used as starting powders to estimate the comparative performance on crack propagation resistance and oxidation behavior according to additional contents of REs. To obtain a reliable relationship between particle size and the deposited morphology of the BCs, the particle sizes of all powders were measured statistically from scanning electron microscopy (SEM) images. Several images were obtained for each type of powder. The projective diameter of an individual particle was measured from SEM images via image processing software (ImageJ, NIH, Bethesda, MD) and was taken as the diameter of the particle. The arithmetic average of the diameter was then calculated and used as the mean diameter of the powder. It was found the oxygen contents in the deposited powders and coatings depended on particle size (Ref 8). With decreasing particle size, the oxygen contents in the just-deposited powders increased exponentially. The oxygen content inside the coating was approximately equal to that in the just-deposited powders for the mean particle size of <50 μm.

Figure 2 shows the typical microstructures of as-sprayed MCrAlY coatings deposited with the powders of CoNiCrAlY (−34.2/+3.8 μm) and 1.5Ce1Si (−45.1/+2.9 μm). They have slightly different particle size ranges and mean values of 11.9 m and 13.3 μm, respectively. But the difference of these two values is relatively so small among the typical commercial spray powders, that the effect of particle size on the seven different types of powders used in this study may be negligible. The oxides in the as-sprayed coatings result from the oxidation of powders, especially from the small-size particles. It can be found that CoNiCrAlY coatings presented a homogeneous structure relative to the others and 1.5Ce1Si, which corresponded to having a narrow particle size range [i.e., the relatively small value of standard deviation (6.8 μm)]. However, all other coatings were deposited by partially melted particles (marked as "1" in Fig. 2b), which correspond to the microstructure of the stacking of the particles in elliptical or near-spherical shapes. Besides the coating fraction deposited by the heavily oxidized particles, the well-flattened lamellae were observed in Fig. 2(b) (marked as "2") and the others. These lamellar coatings were deposited by well-melted particles relatively. The oxygen distribution measured by energy-dispersive x-ray (EDX) analysis illustrates the low oxygen content in the lamellar region (Ref 8). This implies that, even for well-melted particles, oxide formed during the in-flight was mainly distributed over the particle surface. In the case of coatings containing a partially melted particle that is comparable to

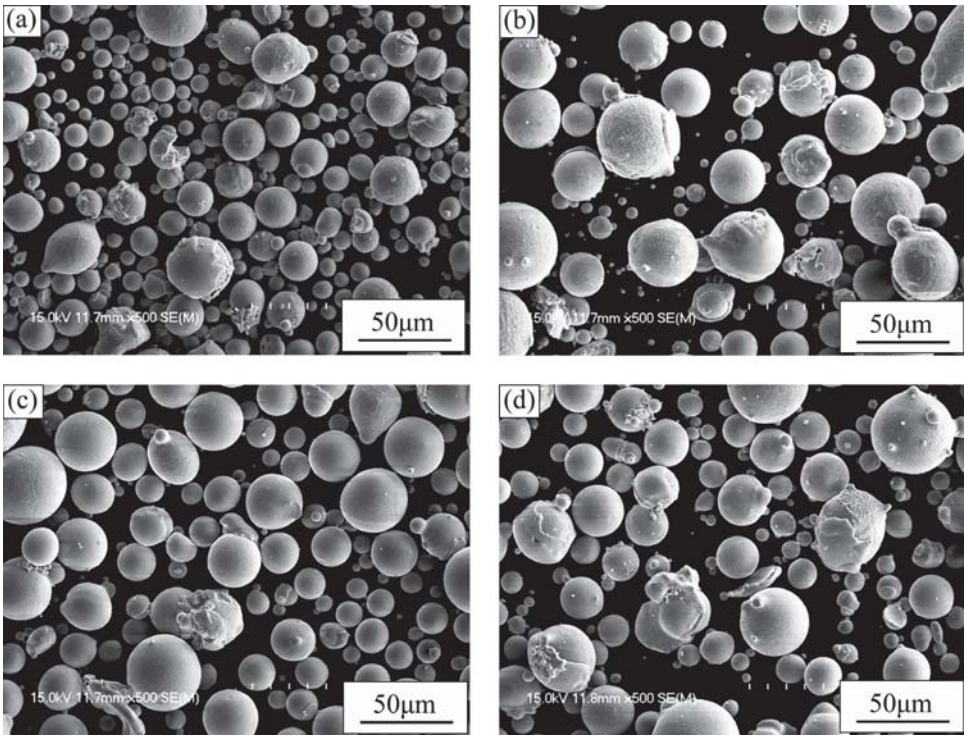

Fig. 1 The morphology of spray powders: (a) CoNiCrAlY (AMDRY 9951); (b) 0.5Ce; (c) 1Si; and (d) 1.5Ce1Si

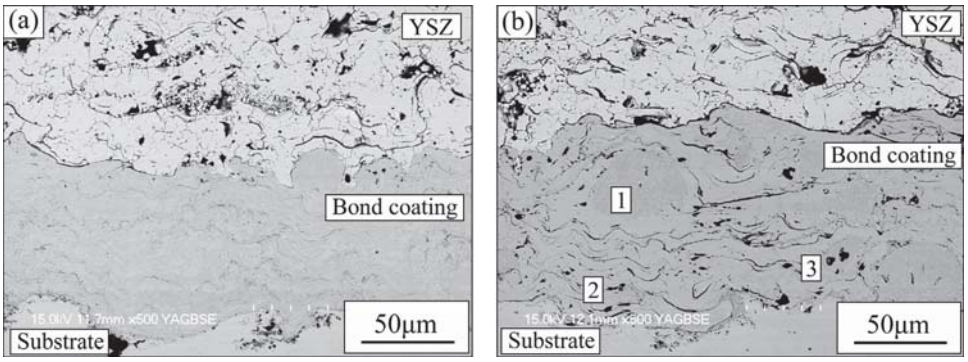

Fig. 2 The morphology of as-sprayed coatings: (a) CoNiCrAlY (AMDRY 9951) and (b) 1.5Ce1Si (1, a partially melted particle; 2, the lamellae; and 3, the internal pores)

well-melted particles, from the distribution of oxygen analysis it is evident that oxygen appeared mainly at the lamellar interface. This fact supports the result that oxide film was covered on the particle surface (Ref 8).

To characterize the oxidation behavior, static oxidation experiments were carried out in air under isothermal conditions at 1373 K for up to 1000 h. After two different exposure times, 100 and 1000 h, the specimens were characterized microstructurally using light optical microscopy and SEM. Each exposure condition consisted of a heating rate of approximately 32 °C/min in a kanthal muffle furnace and an approximately 3 °C/min cooldown to ambient temperature. The specimens were kept in alumina boats, and then the boats were inserted into the furnace. The aim of this oxidation procedure was to create accelerated conditions for testing. After preliminary characterization, the samples were cross sectioned, mounted in transoptic powder, and subjected to mirror polishing to identify the cross-sectional details. The TGO was measured by obtaining a backscattered electron image with a scanning electron microscope, which was attached to a Robinson backscattered detector. The microhardness of the coatings was measured by Fischer microhardness tester (Fischerscope HM2000 Series, Sindelfingen-Maichingen, Germany). A 500 mN load was provided to the needle for penetration, and hardness value was based on the relationship $Hv = 0.1891 \times F/d^2$, where F is the load (in newtons) and d is the mean of the indentation diagonal length (in millimeters).

Figure 3 showed a schematic diagram of the FPB tests. Prior to FPB tests, specimens, which had dimensions of 40 × 5 × 4 mm, were aged for 100 and 1000 h at 1373 K in air. The inner and outer spans of the FPB were 15 and 34 mm, respectively, and

the loading speed was 0.005 mm/s, which is relatively low. During the FPB test, an acoustic emission (AE) sensor and a strain gauge measured AE energy and the compressive strain on the backside of the specimen (i.e., the substrate backside), respectively. Assuming that the starting point of a rapid increase in cumulative AE energy corresponds to the occurrence of the vertical cracking and horizontal delamination, the resistance to crack propagation was evaluated quantitatively by the amount of backside strain at the point of a rapid increase in cumulative AE energy.

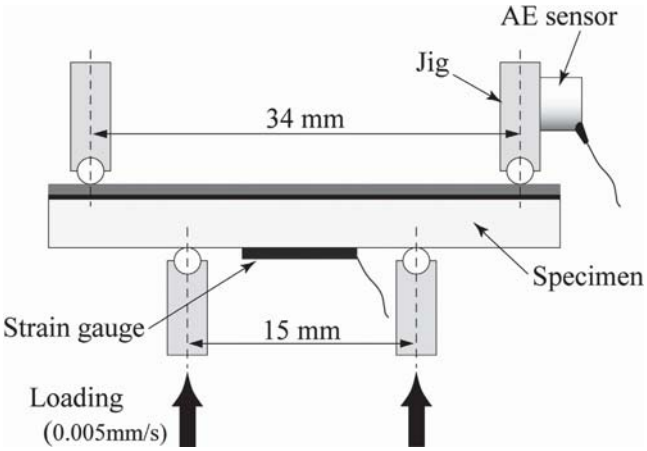

Fig. 3 Schematic diagram of the FPB test

4. Results and Discussion

4.1 High-Temperature Exposure Tests

Cross-sectional SEM observation was performed for the TBC coated with several BCs aged at 1373 K for 100 h. First, to investigate the influence of Ce and Si additions on the oxidation behavior, TGO morphologies at the TC-BC interface were compared with TBC coated with CoNiCrAlY, 1Si, and 0.5Ce BC materials, as shown in Fig. 4. From these images, a continuous Al_2O_3 film was formed mainly at the interface between a YSZ TC and a metallic BC for all samples. In the case of the Si addition (Fig. 4b), the TGO morphology was not changed compared with the TBC coated with conventional CoNiCrAlY (Fig. 4a). In the case of Ce addition, as shown in Fig. 4(c), the TGO morphology was completely different between TBC coated with (Fig. 4c) 0.5Ce BC and the others (Fig. 4a, b). In particular, the formation and the growth of the mixed oxide (gray region in Fig. 4c) were fully developed. In the case of a TBC coated with CoNiCrAlY, the mixed oxides were slightly formed on the Al_2O_3. On the other hand, in TBC coated with 1.5Ce1Si BC material, it seems that the mixed oxides grow into the BC downward to the substrate along the grain boundary in the BC (discussed in section 4.2, see Fig. 7c). That means that the oxide was interwoven with the BC.

Second, to evaluate the effect of the amount of Si, TBCs coated with Si-added BCs using various amounts of Si were compared: Fig. 5(a), 0.5Ce; Fig. 5(b), 0.5Ce1Si; and Fig. 5(c), 0.5Ce2Si. A significant difference was not shown among the

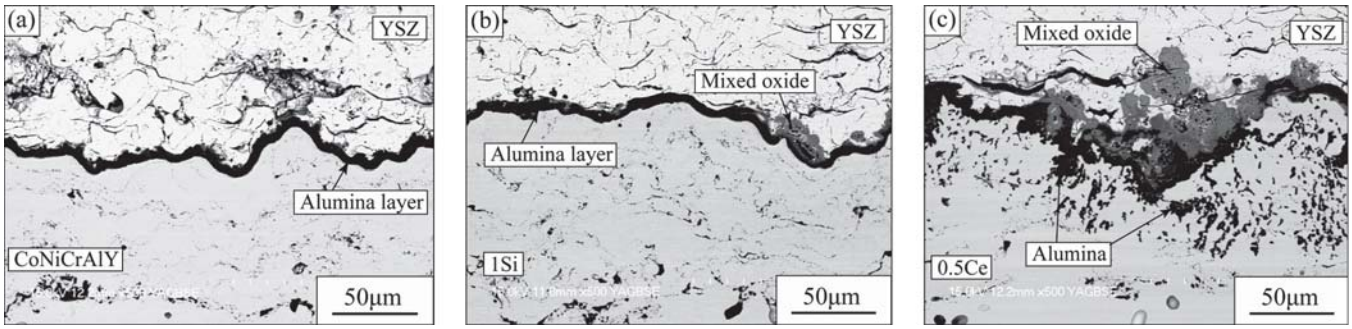

Fig. 4 Cross-sectional SEM images of TBCs aged for 100 h at 1373 K (effects of the separate addition of Si and Ce): (a) CoNiCrAlY; (b) 1Si; and (c) 0.5Ce

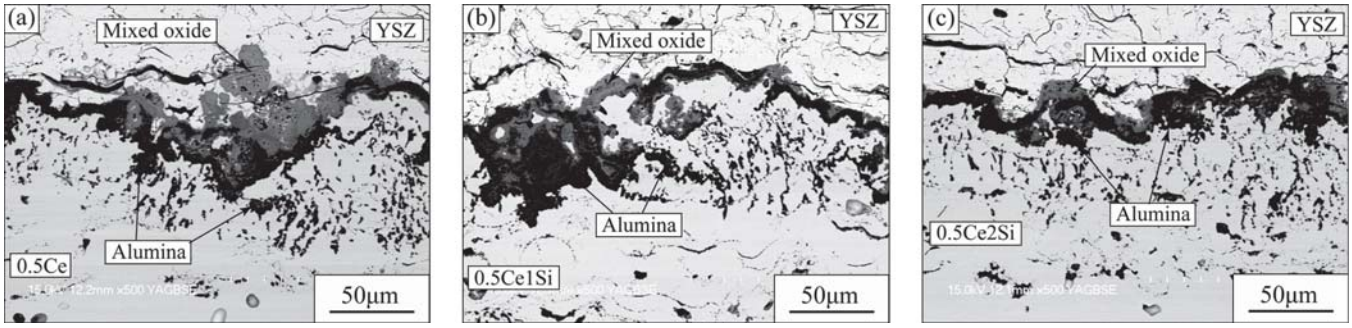

Fig. 5 Cross-sectional SEM images of TBCs aged for 100 h at 1373 K (effects of the variation of Si contents): (a) 0.5Ce; (b) 0.5Ce1Si; and (c) 0.5Ce2Si

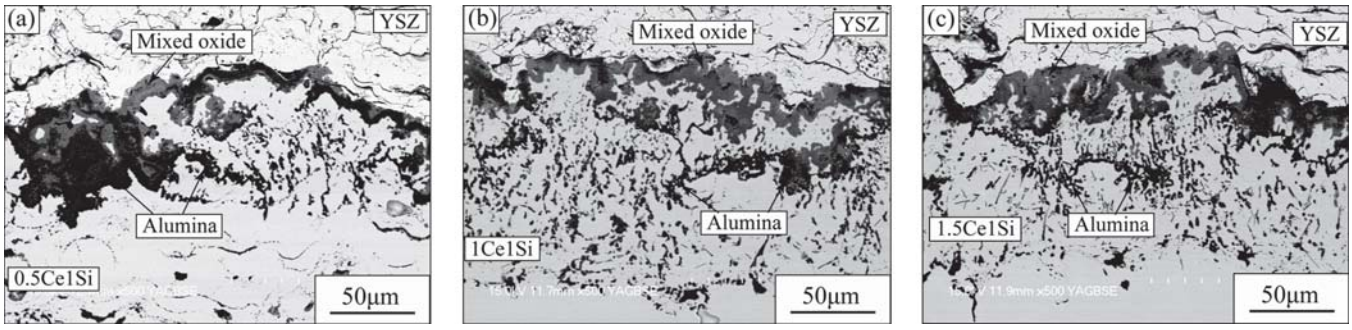

Fig. 6 Cross-sectional SEM images of TBCs aged for 100 h at 1373 K (effects of the variation of Ce contents): (a) 0.5Ce1Si; (b) 1Ce1Si; and (c) 1.5Ce1Si

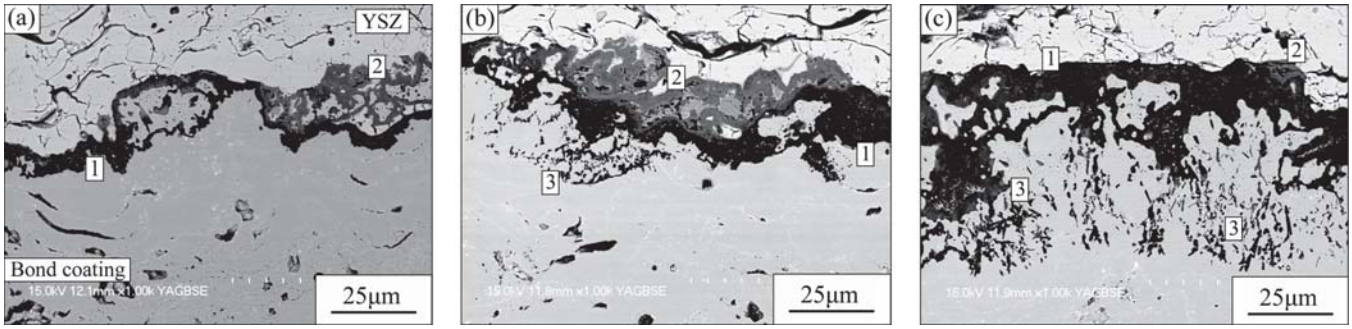

Fig. 7 The growth process of the root-like oxide of TBCs with 1.5Ce1Si BC aged at 1373 K, aged for (a) 1 h (starting the oxidation), (b) 5 h (staring the formation of root-like oxide, and (c) 10 h (the full-developed root-like oxide). 1, alumina; 2, mixed oxide; and 3, root-like oxide regions

three kinds of TBCs with Si-added BCs. The alumina oxide (black region), the mixed oxide (gray region), and internal oxide structures were representative of the entire TC-BC interface region, as shown in Fig. 5. Accordingly, it is thought that there is almost no effect of Si addition on the oxidation behavior. Furthermore, to evaluate the effect of the amount of Ce, TBCs coated with Ce-added BCs using various amounts of Ce were compared: Fig. 6(a), 0.5Ce1Si; Fig. 6(b), 1Ce1Si; and Fig. 6(c), 1.5Ce1Si. From Fig. 6, internal oxide, hereafter called the root-like oxide, was observed close to the interface (downward to the BC below) in all of the panels in Fig. 6. The root-like oxide was accelerated by the addition of >1 wt.% Ce, as shown in Fig. 6(b) and (c). However, there was not much difference between TBCs coated with 1Ce1Si (Fig. 6b) and 1.5Ce1Si (Fig. 6c). From these results, the growth of the root-like oxide was enhanced by the addition of Ce to the conventional CoNiCrAlY. However, it can be thought that the effect may be saturated with the addition of >1 wt.% Ce.

4.2 Mechanisms of Formation of Root-Like Oxide

From SEM observation, the addition of Ce led to the generation of root-like oxide inside the BCs. However, the mechanism of the generation of root-like oxide has not been made clear. The growth process of the root-like oxide was observed regarding a TBC coated with 1.5Ce1Si, as shown in Fig. 7, which showed the most remarkable oxide formation. As a result, the formation of root-like oxide samples aged for 1 h was not observed inside the BC, as shown in Fig. 7(a). However, the root-like oxide started to form after 5 h of aging (marked as "3" in Fig. 7b), and then the oxide thickness was gradually increased. After 10 h of aging, the root-like oxide was completely formed inside the BC (marked as "3" in Fig. 7c). To make clear the mechanism of formation of the root-like oxide, samples aged for 1 and 10 h were observed by EDX. The result of the SEM and EDX analyses are shown in Fig. 8 and 9, respectively. From the SEM image in Fig. 8, there were dark gray and white regions. In the dark gray regions (marked as "1"), mainly Al and Ni were identified. Therefore, the dark gray regions can be NiAl intermetallic, namely β phase. On the other hand, in the white regions (marked as "2" and "3"), Al, Ce, Y, and O were identified by EDX analysis. From this result, Ce oxide (supposed to be CeO_2 at point 2) and Al-Ce-Y oxide (supposed to be CeO_2 at point 3) already existed inside the BC at this point. But Al-Ce-Y oxides can be seen only at the points overlapped with Ni-Al signals (see other overlapping points between the dark gray and white regions in Fig. 8). Point 2 has only a Ce-O signal without overlapping, making it possible that the Ce oxide formed first with the Ni-Al intermetallic spreading to the Ce oxide region gradually, so Al-Ce-Y-O overlapping happens. Other elements also can diffuse to Ce oxides with long exposure time (i.e., the Si-Ce-Y oxides and Al-Ce-Y oxides can be seen in Fig. 9 at points 1 and 2, respectively). This result can lead us to suppose that Ce oxidized preferentially rather than Al. From the Ellingham diagram, Al, rather than Ce, oxidized preferentially at 1373 K. However, in this case, opposite result was obtained. The following reasons can be considered:

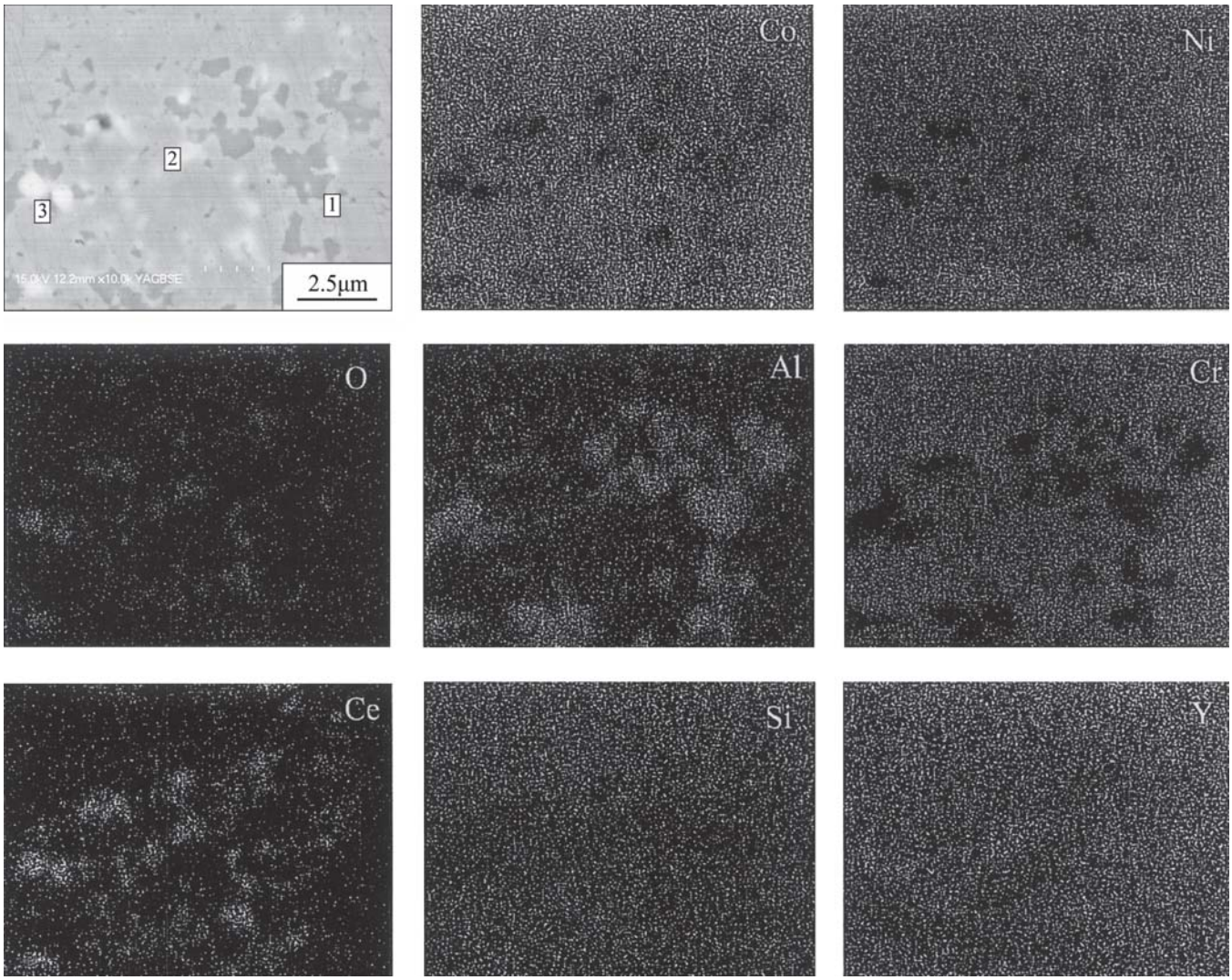

Fig. 8 EDX analysis of 1.5Ce1Si TBC aged for 1 h at 1373 K: 1, Ni-Al; 2, Ce-O; and 3, Al-Ce-Y-O compounds

- Al makes the intermetallic with Ni. The intermetallic is relatively stable. Therefore, Al cannot be easy to oxidize.
- The solid solubility limit of Ce in CoNiCrAlY is very low. There is a possibility that Ce, which exceeded the solid solubility limit, independently segregated.

And the Ce oxide, which was observed inside the BC in the sample aged for 1 h, can affect the oxidation behavior of the BC. It is known about characteristics of Ce-oxide as follows:

- Ce oxide has a higher diffusion rate than Al_2O_3.
- Diffusion rate of O into Al_2O_3: D_{Al2O3}, $10^{-15} \sim 10^{-27}$ m^2/s (1273 K) (Ref 9)
- Diffusion rate of O into CeO_2: D_{CeO2}, $10^{-8} \sim 10^{-12}$ m^2/s (1373 K) (Ref 10)
- Diffusion rate of Al into MCrAlY (12 wt.%Al): D_{Al}, 10^{-14} m^2/s (1373 K) (Ref 11).
- Ce has a nonstoichiometric property and an oxygen storage function.

$$CeO_2 \leftrightarrow CeO_{2-x} + \frac{x}{2} O_2$$

From these characteristics, it is suggested that Ce oxide can be an oxygen path in BCs.

In the case of samples aged for >5 h, the NiAl intermetallic (β phase) did not observe inside the BC. This means that Al in NiAl oxidized as Al_2O_3. As a result, it can be deduced that the Al concentration gradient between the interface and the inside of the BC is due to the decreasing Al concentration in the BC. Furthermore, focusing on the Al_2O_3 at the interface, the Al_2O_3 was a porous film. Generally, the Al_2O_3 was dense and should play the role of oxygen barrier. However, in this case, it can be easy for oxygen to penetrate via such porous Al_2O_3. From the result of observations of the specimen aged for 1 h, Ce oxide was formed on a diffusion path for oxygen in the BC. Therefore, the Al, which remained in the BC, was oxidized on the inside of the BC. From the results, it has been suggested that the oxidation mechanism of the BC in the case of TBC coated

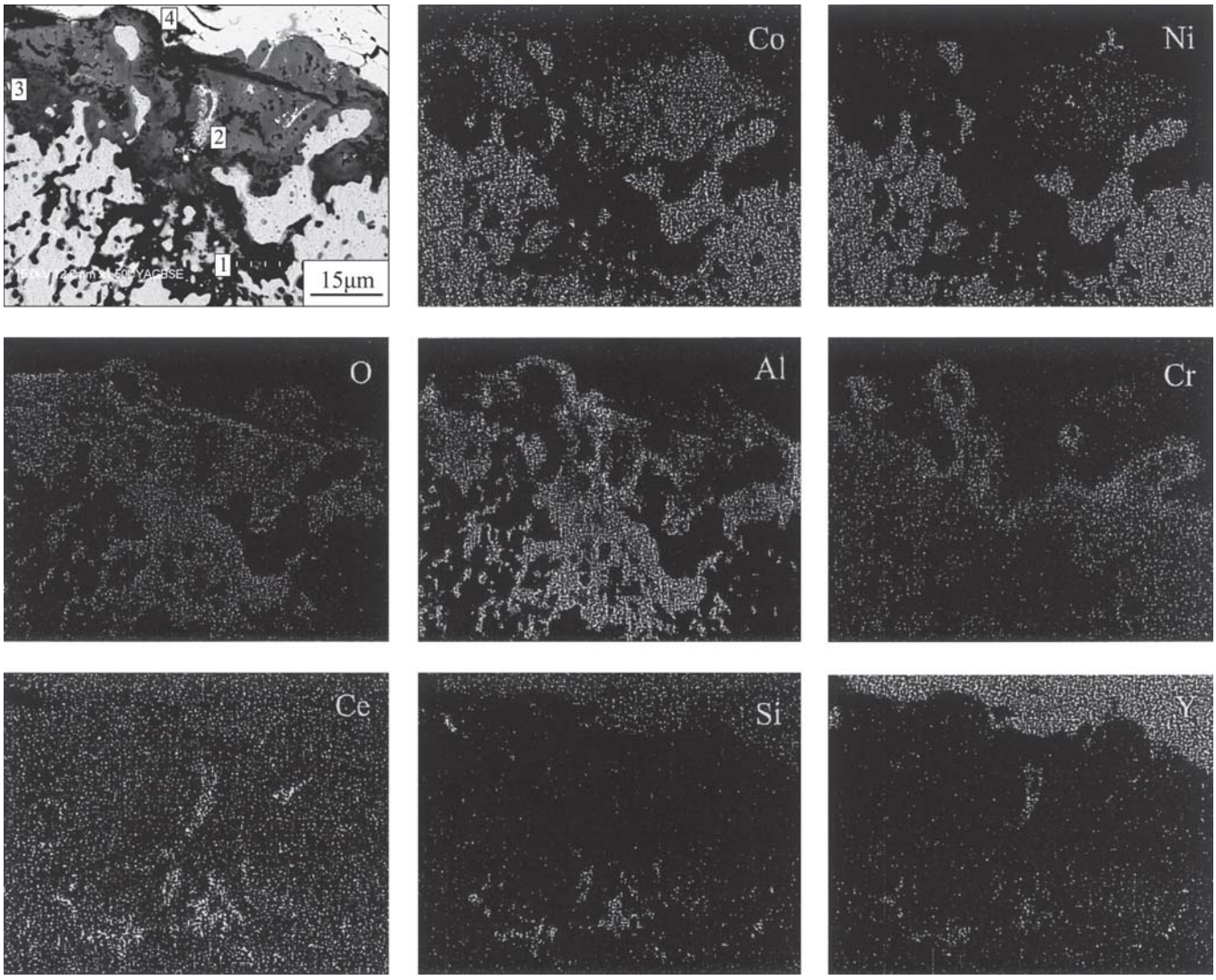

Fig. 9 EDX analysis of 1.5Ce1Si TBC aged for 100 h at 1373 K: 1, Si-Ce-Y-O; 2, Al-Ce-Y-O; 3, Al-O; and 4, Cr-Al-O compounds

with Ce-added BC. The schematic illustration of the TGO formation mechanism is shown in Fig. 10.

Due to high-temperature exposure, first, the Ce in the BC was oxidized. And then, Al_2O_3 was formed at the interface between the TBC and the BC. If there is NiAl intermetallic (β phase) in the BC, the diffusion of Al to the interface and the growth of Al_2O_3 proceed due to the existence of the Al concentration gradient. When the β phase depleted, the diffusion rate of Al to the interface can decrease. And then, due to the formation of a porous Al_2O_3 layer at the interface, it is easy for oxygen to penetrate to the inside of the BC. Moreover, oxygen penetrates deeper through the Ce oxide. As a result, the root-like oxides can be formed.

4.3 Effect of Sintering Kinetics on Crack Propagation

It is now fairly clear that a major reason for the relatively high thermomechanical stability of plasma-sprayed zirconia TCs is that their macroscopic stiffness is low, so that residual stress levels remain relatively low and the material has a high strain tolerance. This apparently arises because, while the local stiffness may be close to that for dense material, the presence of defects (e.g., microcracks, pores, and lack of intersplat bonding) ensures that the global value is low, although it is expected to rise under compressive stresses that are large enough to cause, for example, the closure of microcracks. The TCs produced by electron beam physical vapor deposition also have a relatively low stiffness, attributable predominantly to poor intercolumnar contact. However, it is starting to become clear (Ref 9-14) that the stiffness of the TC can rise appreciably under service conditions, because at least some of the defects start to sinter and heal. This is likely to raise the residual stress levels and associated strain energy release rate, making spallation more likely. There is, however, a severe shortage of definitive data in this area and of mechanistic explanations for the observed changes. The Young's modulus of as-sprayed material, as measured by the cantilever bend test, was found to be about 10 GPa. This is in

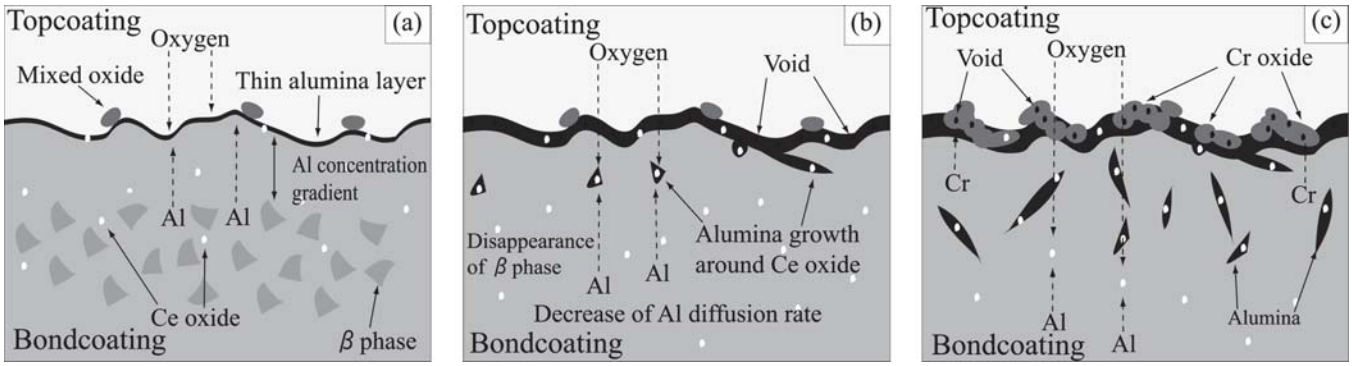

Fig. 10 Schematic illustration of the root-like oxide formation mechanism (in the case of a TBC with Ce-added BC aged at 1373 K for (a) 1 h, (b) 5 h, and (c) 10 h

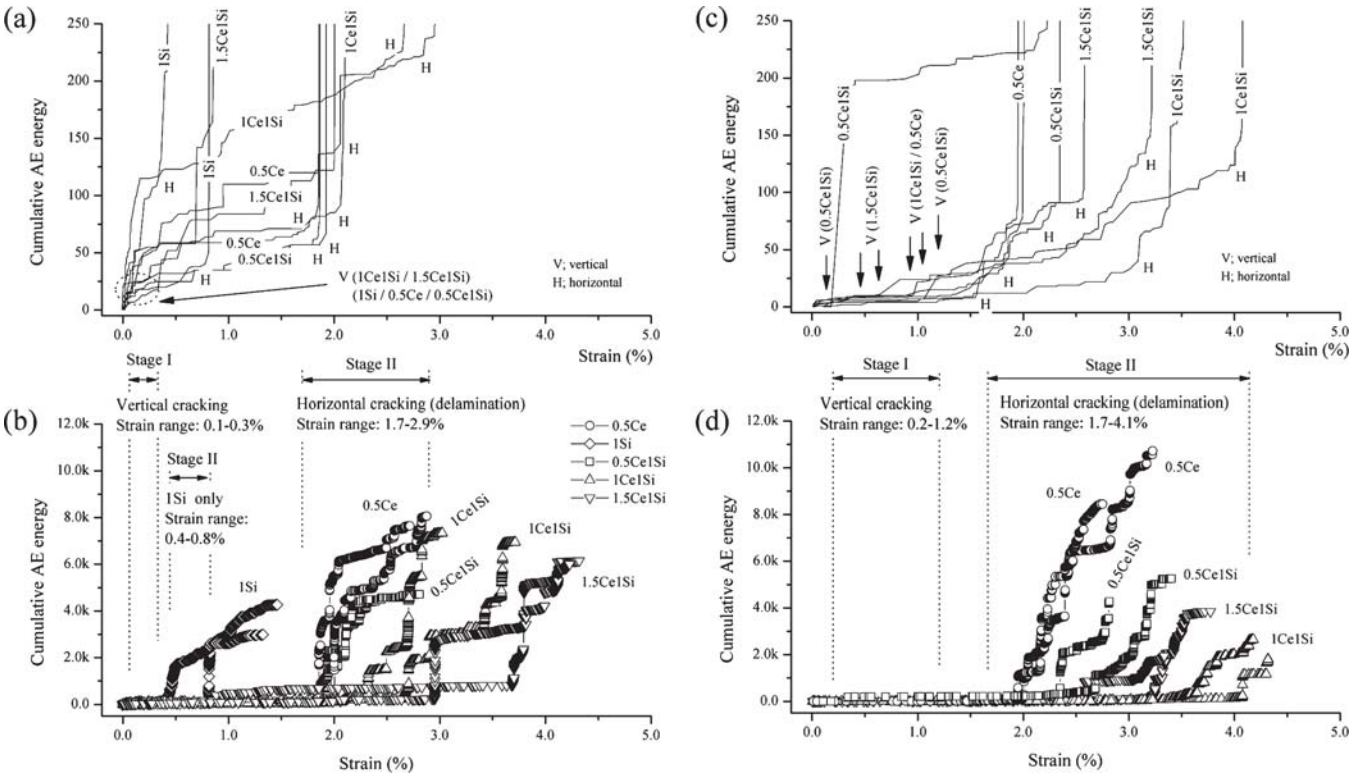

Fig. 11 The results of FPB tests for the TBCs at 1373 K: (a, b) aged for 100 h; and (c, d) aged for 1000 h. (a) and (c) are detailed graphs rescaled in low-AE energy level for (b) and (d), respectively. TBCs with CoNiCrAlY were delaminated during 100 and 1000 h aging. The 1Si-added TBC was also delaminated during 1000 h of aging. These cases are omitted in the graphs.

good general agreement with some data in the literature, at least for studies using measurement techniques that are sensitive to the global stiffness of the material (Ref 15, 16). The value is considerably lower than that of bulk zirconia (200–220 GPa). This reduction is attributed to the presence of defects, particularly the high density of through-thickness microcracks. These cracks form during deposition, as the molten splats freeze and cool to the substrate temperature. Thermal contraction results in tensile stresses within the splat, causing through-thickness intrasplat cracking. Poor bonding between splats is also common, as shown in Fig. 11(a) (Ref 17).

In general, it is global (volume-averaged) values that will determine the stress levels arising from the imposition of strain (such as will result from the differential thermal contraction between the substrate and the coating). There are, however, further points of interest. In tension, microcracks will open, and some intersplat shear is also likely to occur. The tensile strain is largely accommodated by the operation of these two mechanisms. However, half of the beam experiences compressive loading. Up to a certain strain, the displacement will largely be accommodated by microcrack closure and by intersplat shear. At sufficiently high compressive strains, however, the micro-

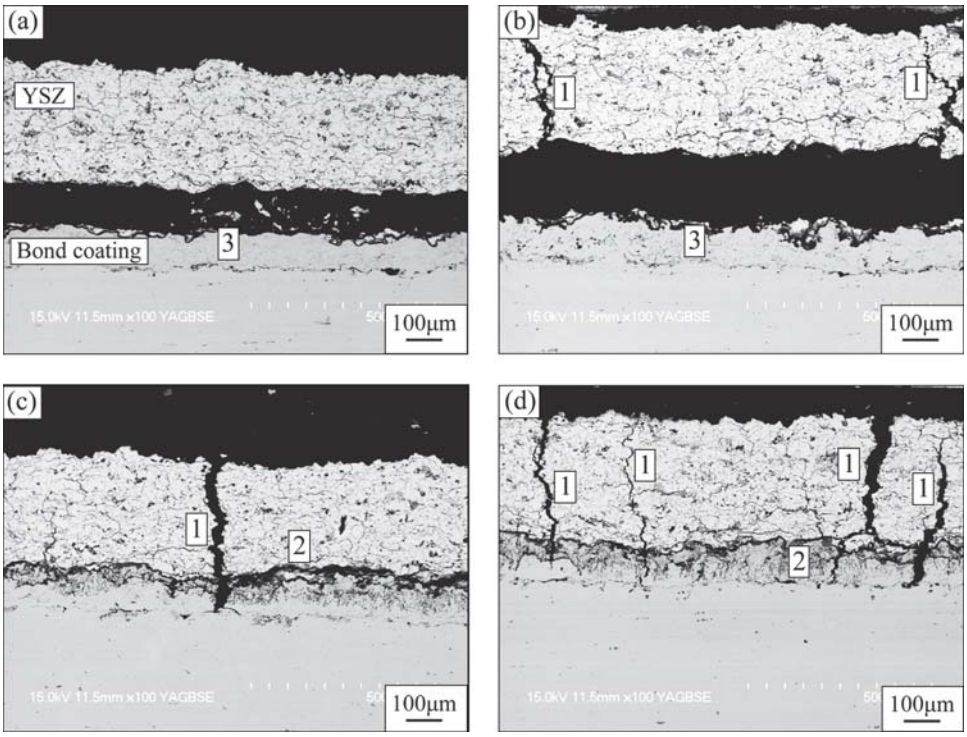

Fig. 12 Crack propagation of TBCs aged for 100 h at 1373 K after FPB tests for (a) 1Si, (b) 0.5Ce1Si, (c) 1Ce1Si, and (d) 1.5Ce1Si. 1, vertical crack; 2, horizontal crack; and 3, interfacial delamination at the TC-BC interface

cracks will become fully closed. Intersplat shear displacement might be expected to operate similarly under compression and tension, but because many intersplat interfaces will be inclined at some angle to the stress axis, a normal compressive stress will develop across them under compressive loading, which would tend to inhibit this shear. As a result of these two effects, the modulus is expected to increase sharply as the compressive strain rises (Ref 17). Intersplat spacings can be even smaller than microcrack openings, but because they are often inclined at only relatively small angles to the plane of the coating, the development of significant normal compressive stress across them is unlikely to occur at lower macroscopic in-plane strains than this.

Sharp changes in stiffness after short sintering times have also been observed by Eaton and Novak (Ref 10). While pronounced sintering of zirconia powders is not in general expected at temperatures below approximately 1673K, Wesling and Socie (Ref 16) have reported detectable effects in plasma-sprayed zirconia at temperatures as low as 1073 K. A study of the associated microstructural changes reveals the mechanisms responsible for these effects. The free surfaces and fractured edges from a sample aged at 1373 K for 114 h are shown in Fig. 11(b). These may be compared with the corresponding views of as-sprayed samples presented in Fig. 11(a). While the free surface shows no evidence of significant changes to the microcrack structures, it can be seen in Fig. 11(b) that grain growth and the associated improvements in bonding and coherence have occurred across the splat boundary. This is expected to raise the stiffness appreciably, although the continued presence of the microcracks will ensure that it remains relatively low. In contrast, samples aged at 1573 K for 114 h show evidence of both improved intersplat bonding and microcrack healing. The second stage of stiffening, in which a progressive rise is observed at the higher heat treatment temperatures, is therefore attributed to repair of the microcracks. The two stages in the sintering process are shown schematically in Fig. 12 (Ref 17). However, even after such treatments, the coating is by no means fully dense, and much intersplat porosity remains. Grain growth across splat boundaries appears to require that the splats be in fairly intimate contact, so that relatively large pores formed, for example, near the splat edges, tend to persist. In fact, the overall porosity levels, as measured by densitometry, remained fairly constant at about 12 to 15% throughout these treatments.

It is of interest to consider what stiffness level will be approached after very long periods at different temperatures. It might be expected that extended exposure to temperatures that are sufficient to heal cracks and lock splats together would lead to material of a stiffness similar to that of bulk material containing approximately 12 to 15% of spherical voids. Application of the Eshelby model yields a value of approximately 150 GPa for such material. It can be seen that values as high as this were not approached during these experiments (Ref 17). This suggests that the complete repair of microcracks may be a difficult process and also that the spheroidization of pores is very slow. Data for stiffness as a function of annealing time and temperature, with the heat treatments carried out while the TC remained attached to the substrate, were examined by Thompson and Clyne (Ref 17). On comparing these data with those in bending tests of detached TCs, it is clear that not only has the presence of the substrate reduced the rate of TC stiffening, but the heat treatment has generated a reduction in the Young's modulus after treat-

ment at low temperature and for short times at the higher temperature (1273 K). This is attributable to the effect of the stress state in the TC during the heat treatment. The higher thermal expansivity of the substrate ensured that the TC was under significant tension at the heat treatment temperature, so that the microcracks were held open. One consequence of the low stiffness (10 GPa) of the as-sprayed TCs is that the stress levels in them (arising during spraying, and during subsequent heating and cooling while attached to the substrate) tend to remain relatively low. As noted above, heating from room temperature to a service temperature might typically generate 4 millistrain, so that, if this were accommodated entirely within the TC, the corresponding stress would be about 40 MPa. The corresponding strain energy release rates (for debonding at the BC-TC interface) therefore also tend to be relatively low, and this is largely responsible for the good thermomechanical stability exhibited by these TBC systems.

The stiffness increases generated by specific heat treatments were found to be considerably reduced if they were carried out while the TC remained attached to the substrate (and the BC), as shown Table 2. The elastic modulus values are increased after heat exposure due to the sintering effect, as mentioned above, but there is no difference between the values of the samples aged for 100 and 1000 h. But the microhardness values are decreased with increasing exposure time. In fact, for relatively low treatment temperatures, it was found that the stiffness could decrease slightly during the treatment. This is attributed to the effect of differential thermal expansion setting up tensile stresses in the TC at elevated temperatures. These stresses, which were typically around 40 MPa in the work described here (Ref 17), are thought to open up microcracks and intersplat boundaries, retarding the sintering process and/or locking the microstructure into a more open configuration. It is also likely that the tensile stresses create new microcracks and other defects, contributing to the drop in stiffness.

4.4 Crack Propagation Resistance Under Pure Bending Load

Figure 13(a) and (b) show the FPB results of specimens, used in this study, that were aged for 100 and 1000 h, respectively, at 1373 K. During the FPB test in this study, there are two types of cracks: vertical cracks move downward from the free TC surface to the BC inside (stage I); and horizontal cracks (delamination) propagate toward the TC-BC interfaces (stage II). In this study, the starting point of stage II is considered to be the criterion level of the comparative performance to the crack resistance under FPB loading.

In the case of TBC coated with the conventional CoNiCrAlY, delamination at the TC-BC interfaces occurred during heat treatment. Accordingly, this specimen could not be tested. This result shows that the TBC coated with the conventional CoNiCrAlY has low crack resistance under FPB loading. In the case of specimens aged for 100 h (Fig. 13a), the delamination points delayed with increasing Ce addition to the BC (i.e., the resistance to crack propagation increased). In samples aged for 1000 h, TBC coated with 1Si was delaminated only during high-temperature exposure before testing. As a result, the addition of Si cannot be effective for the improvement of crack resistance. And the TBC coated with 1Ce1Si showed the highest delamination resistance (Fig. 13c, d). In this specimen, the strain value of the starting point of delamination was approximately 4%. This indicates the effect of the addition of Ce. In the case of Ce added to TBC samples, the delamination start points (stage I and II) were de-

Table 2 Microhardness and elastic modulus of TBCs at 1373 K as a function of exposure time

	Microhardness, HV			Elastic modulus, GPa		
Designation	**As-sprayed**	**100 h**	**1000 h**	**As-sprayed**	**100 h**	**1000 h**
CoNiCrAlY	360.6	368.4	267.3	141	201.1	201.8
0.5Ce	535.8	290	201.1	160	214.7	218
1Si	551.1	368.8	208.8	141.9	216.4	202
0.5Ce1Si	527.3	299.4	221.3	133.8	186.4	222.1
1Ce1Si	538	286.9	208.7	135.2	226.4	220.9
1.5Ce1Si	573.7	241.6	217.2	135.6	222.2	225.2
0.5Ce2Si	547.4	261.2	206.3	128.3	206	221.5

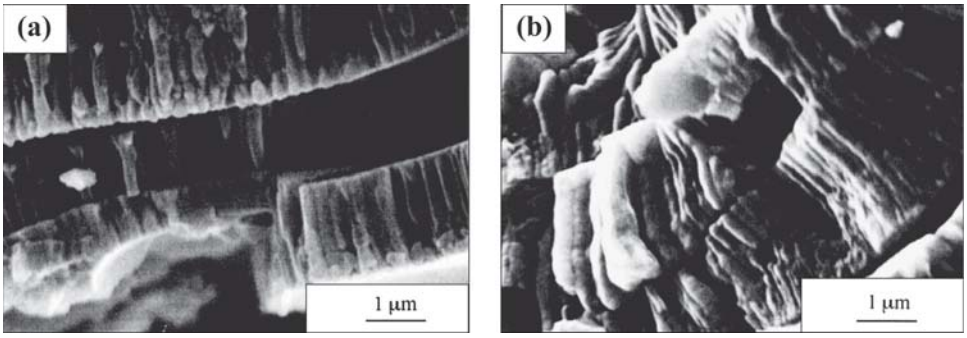

Fig. 13 SEM micrographs of TC materials on a transverse fracture surface: (a) as-sprayed (poor intersplat bonding); and (b) after a heat treatment of 114 h at 1373 K (improved in intersplat bonding) (Ref 16)

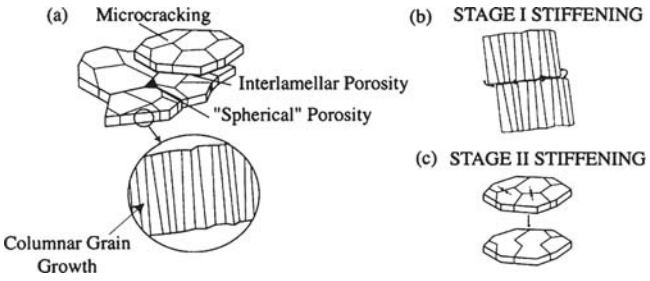

Fig. 14 Schematic depiction of the microstructural defects present in as-sprayed coatings and of the healing processes that occur during heat treatment and give rise to the observed two-stage stiffening (Ref 16)

layed for conditions of aging for both 100 and 1000 h. Both the vertical and horizontal crack resistances were improved with Ce addition under heat exposure. When the Ce included was >1 wt.%, the effect of Ce addition can be saturated. Normally, due to degradation, the start point of crack propagation (stage I and II) gradually advances with the heat exposure time. Therefore, it was supposed that the TBCs aged for 1000 h had a lower crack resistance than those aged for 100 h. However, due to the sintering effect in the coated layers, as mentioned above, the crack resistance did not drop.

To clarify the mechanism of the improvement of crack resistance in TBCs, cross-sectional SEM images of the tested specimens were observed, as shown in Fig. 14. In the case of the TBCs coated with a low Ce-added BC (Fig. 14a, b), the delamination to failures were mainly observed in the vicinity of the interface. On the other hand, in TBCs with relatively high Ce-added BC (Fig. 14c, d), the vertical cracks formed inside the TC and the BC, and the horizontal microcracks were formed at the TC-BC interfaces. But any cracks did not lead to the delamination to failures. From Fig. 5 to 7, the Ce addition to the BC drastically changed the TGO morphologies, namely, the formation of root-like oxides. The root-like oxides can improve the resistance of crack propagation in this case. It is supposed that the reason of the improvement is an anchor effect.

5. Conclusions

In this study, to promote the improvement of crack resistance at the interface between the TBC and the BC, Ce and Si elements were added to the conventional CoNiCrAlY powders. The following conclusions can be drawn:

- By adding Ce and Si to conventional CoNiCrAlY, the morphologies of TGO changed drastically. Furthermore, the influence became more pronounced when the amount of Ce increased.
- The addition of Si to the conventional CoNiCrAlY BC cannot be effective for the improvement of TGO morphology and crack resistance under pure bending load.
- The resistance of crack propagation increased with increasing Ce addition to the BC. Therefore, Ce addition can be effective for the improvement of crack resistance.
- In the case of TBCs exposed to high temperature, crack resistance was improved due to the sintering effect of the overlayers.
- The addition of Ce to the BC made the root-like oxides. The root-like oxide can improve crack resistance under pure bending load. It is supposed that the reason for this improvement is an anchor effect.

References

1. S.M. Meier and D.K. Gupta, The Evolution of Thermal Barrier Coatings in Gas Turbine Engine Applications, *Trans. ASME,* 1994, **116,** p 250-257
2. B.J. Gill and R.C. Tucker Jr., Plasma Spray Coating Process, *Mater. Sci. Technol.,* 1986, **2,** p 207-213
3. K. Ogawa, T. Shoji, H. Aoki, N. Fujita, and T. Torigoe, Mechanistic Understanding for Degraded Thermal Barrier Coatings, *Mater. Eng. A,* 2001, **44**(4), p 507-513
4. G.M. Newaz, S.Q. Nusier, and Z.A. Chaudhury, Damage Accumulation Mechanisms in Thermal Barrier Coatings, *Trans. ASME,* 1998, **120**(2), p 149-153
5. K. Ogawa, T. Kato, and T. Shoji, Improvement of Interface Bonding Strength Between Ceramic Thermal Barrier Coatings and Metallic Bond-Coats, *International Thermal Spray Conference,* E. Lugscheider and C.C. Berndt, Ed., March 4-6, 2002 (Essen, Germany), DVS Deutscher Verband für Schweissen, 2002, p 900-904
6. H. Choi, B. Yoon, H. Kim, and C. Lee, Isothermal Oxidation of Air Plasma Spray NiCrAlY Bond-Coats, *Surf. Coat. Technol.,* 2002, **150,** p 297-308
7. M. Tanno, K. Ogawa, and T. Shoji, Effect of Cerium and Silicon Additions to MCrAlY on the High-Temperature Oxidation Behavior and Bond Strength of Thermal Barrier Coatings, *Key Eng. Mater.,* 2004, **261-263,** p 1062-1066
8. C.J. Li and W.Y. Li, Effect of Sprayed Powder Particle Size on the Oxidation Behavior of MCrAlY Materials During High Velocity Oxygen-Fuel Deposition, *Surf. Coat. Technol.,* 2002, **162**(1), p 31-41
9. D.M. Zhu and R.A. Miller, Thermal Conductivity and Elastic Modulus Evolution of Thermal Barrier Coatings Under High Heat Flux Conditions, *J. Thermal Spray Technol.,* 2000, **9**(2), p 175-180
10. H.E. Eaton and R.C. Novak, Sintering Studies of Plasma-Sprayed Zirconia, *Surf. Coat. Technol.,* 1987, **32**(1-4), p 227-236
11. H.C. Chen, E. Pfender, and J. Heberlein, Structural Changes in Plasma-Sprayed ZrO_2 Coatings After Hot Isostatic Pressing, *Thin Solid Films,* 1997, **293**(1-2), p 227-235
12. D.M. Zhu and R.A. Miller, Sintering and Creep Behavior of Plasma-Sprayed Zirconia- and Hafnia-Based Thermal Barrier Coatings, *Surf. Coat. Technol.,* 1998, **108-109**(1-3), p 114-120
13. B.Z. Janos, E. Lugscheider, and P. Remer, Effect of Thermal Aging on the Erosion Resistance of Air Plasma Sprayed Zirconia Thermal Barrier Coating, *Surf. Coat. Technol.,* 1999, **113**(3), p 278-285
14. J. Ilavsky, G.G. Long, A.J. Allen, and C.C. Berndt, Evolution of the Void Structure in Plasma-Sprayed YSZ Deposits During Heating, *Mater. Sci. Eng. A,* 1999, **272**(1), p 215-221
15. H. Ibegazene, S. Alperine, and C. Diot, Yttria-Stabilized Hafnia-Zirconia Thermal Barrier Coatings: The Influence of Hafnia Addition on TBC Structure and High-Temperature Behaviour, *J. Mater. Sci.,* 1995, **30**(4), p 938-951
16. K.F. Wesling and D.F. Socie, Fatigue of Thick Thermal Barrier Coatings, *J. Am. Ceram. Soc.,* 1994, **77**(7), p 1863-1868
17. J.A. Thompson and T.W. Clyne, The Effect of Heat Treatment on the Stiffness of Zirconia Top Coats in Plasma-Sprayed TBCs, *Acta Mater.,* 2001, **49**(9), p 1565-1575